THE JOURNAL OF BIOLOGICAL CHEMISTRY
Vol. 279, No. 33, Issue of August 13, pp. 34833–34839, 2004
Printed in U.S.A.

Solution Structure of Cox11, a Novel Type of β-Immunoglobulin-like Fold Involved in Cu_B Site Formation of Cytochrome *c* Oxidase*[S]

Received for publication, April 2, 2004, and in revised form, May 26, 2004
Published, JBC Papers in Press, June 4, 2004, DOI 10.1074/jbc.M403655200

Lucia Banci‡, Ivano Bertini‡§, Francesca Cantini‡, Simone Ciofi-Baffoni‡, Leonardo Gonnelli‡, and Stefano Mangani¶

From the From ‡Magnetic Resonance Center CERM and Department of Chemistry, University of Florence, Via Luigi Sacconi 6, 50019, Sesto Fiorentino, Florence, Italy and ¶Department of Chemistry, University of Siena, Via Aldo Moro, 53100, Siena, Italy

Cytochrome *c* oxidase assembly process involves many accessory proteins including Cox11, which is a copper-binding protein required for Cu incorporation into the Cu_B site of cytochrome *c* oxidase. In a genome wide search, a number of Cox11 homologs are found in all of the eukaryotes with complete genomes and in several Gram-negative bacteria. All of them possess a highly homologous soluble domain and contain an N-terminal fragment that anchors the protein to the membrane. An anchor-free construct of 164 amino acids was obtained from *Sinorhizobium meliloti*, and the first structure of this class of proteins is reported here. The apoform has an immunoglobulin-like fold with a novel type of β-strand organization. The copper binding motif composed of two highly conserved cysteines is located on one side of the β-barrel structure. The apoprotein is monomeric in the presence of dithiothreitol, whereas it dimerizes in the absence of the reductant. When copper(I) binds, NMR and extended x-ray absorption fine structure (EXAFS) data indicate a dimeric protein state with two thiolates bridging two copper(I) ions. The present results advance the knowledge on the poorly understood molecular aspects of cytochrome *c* oxidase assembly.

Cytochrome *c* oxidase (CcO)[1] is the terminal enzyme in the electron transport system, reducing oxygen to water and generating the proton gradient that drives ATP synthesis. Multiple subunits and several cofactors are necessary for catalytic activity including two hemes *a*, a magnesium ion, a zinc ion, and three copper ions. In particular, the copper ions are located in subunits COX I and COX II, which contain the Cu_B and Cu_A centers, respectively. The insertion of these cofactors and assembly of the CcO complex in the inner mitochondrial membrane requires accessory proteins (for a general review, see Ref. 1). It has recently become clear that the required metal ions cannot simply diffuse to the requisite compartment of the cell for insertion into the desired protein, but a complex machinery of metal importers and chaperones is required (2). In eukaryotes, two metallochaperones, Cox17 and Cox19, were proposed to shuttle copper in the mitochondrion (3, 4). Other nuclear genes also are required for the proper insertion of copper into CcO (5–8). In particular, it is well established that a mitochondrial inner membrane protein, Sco1, interacting with COX II subunit (9), is important for copper insertion into the binuclear Cu_A site (10, 11). On the contrary, the process through which copper is provided to COX I subunit, which contains a copper ion buried 13 Å below the membrane surface, still remains essentially obscure, even if it is known that it requires another mitochondrial inner membrane protein, Cox11. Cox11 was first shown to be implicated in the CcO maturation process from the observation that Δ*cox11* yeast lacked CcO activity and was deficient in heme *a* (5). It was also observed that, for *cox11* mutants lacking CcO activity, RNA and protein synthesis of the core subunits I and II are normal, suggesting that Cox11 functions post-translationally to generate active CcO (5). However, it is now evident that other two proteins rather than Cox11 are the key enzymes involved in heme *a* formation (12, 13). More recently, it was indeed demonstrated that the Cu_B site is absent in CcO purified from *Rhodobacter sphaeroides* lacking *cox11* (14). These results suggest that Cox11 functions primarily in Cu_B site formation, possibly delivering copper directly to that site. Alternatively, Cox11 could act as a co-chaperone, facilitating Cu(I) donation through another molecule. In particular, Cox11 may function in copper insertion with specificity for Cu_B site in a fashion analogous to that hypothesized for the metallation of the Cu_A site, *i.e.* Cox17 donates Cu(I) to Sco1, which inserts copper into the Cu_A site (1).

In yeast Cox11, a 34-kDa protein anchored by a single transmembrane segment to the inner mitochondrial membrane, the soluble C-terminal domain is in a dimeric state both in the apoform and Cu(I) bound form (15). The protein binds one copper atom per monomer, and from the EXAFS data, it was observed that the two copper ions are in close proximity (15). It was suggested that copper is coordinated by three conserved cysteine residues, even if it was not possible to determine whether they all belong to the same subunit of the dimer or if one of them belongs to the other subunit (15). Mutation of any of these Cys residues reduces Cu(I) binding and confers respiratory incompetence and reduced CcO activity (15).

In this study, we browsed GenBank™ to search for homologs of yeast Cox11 in prokaryotic organisms and we selected five sequences, cloned them, and expressed them in a high throughput approach. We then have solved the three-dimensional so-

* This work was supported by the European Community (SPINE Grant QLG2-CT-2002-00988, "Structural Proteomics in Europe"), by Ente Cassa Risparmio di Firenze, and by Ministero dell'Istruzione dell'Universitá e della Ricerca. The costs of publication of this article were defrayed in part by the payment of page charges. This article must therefore be hereby marked "*advertisement*" in accordance with 18 U.S.C. Section 1734 solely to indicate this fact.

[S] The on-line version of this article (available at http://www.jbc.org) contains Supplemental Figs. 1–6 and Tables 1–4.

§ To whom correspondence should be addressed: CERM and Department of Chemistry, University of Florence, Via L. Sacconi 6, Sesto Fiorentino 50019, Italy. Tel.: 39-055-4574272; Fax: 39-055-4574271; E-mail: ivanobertini@cerm.unifi.it.

[1] The abbreviations used are: CcO, cytochrome *c* oxidase; DTT, dithiothreitol; MES, 4-morpholineethanesulfonic acid; NOE, nuclear Overhauser effect; XAS, X-ray absorption spectroscopy; EXAFS, extended x-ray absorption fine structure.

lution structure of the soluble C-terminal domain of Cox11 from *Sinorhizobium meliloti* (in the metal-free form, it is purified) to further address, on the basis of the structural properties, its role in the assembly of the Cu_B center of CcO. The soluble domain of apoCox11 adopts a novel type of β-immunoglobulin (Ig)-like fold. The interaction with copper(I) was investigated by EXAFS spectroscopy. It comes out that an immunoglobulin-fold can be adapted to bind copper(I) with sulfur atoms in a dimeric structural arrangement that involves a binuclear copper(I) cluster. The structural findings then are discussed on the basis of the mechanistic implication of Cox11 in the Cu_B site formation.

EXPERIMENTAL PROCEDURES

Sequence Search and Analysis—Cox11 sequences were searched in all of the non-redundant GenBank™ databases (coding sequences translations + Protein Data Bank + Swiss-Prot + Protein Information Resource + Protein Research Foundation) using sequence similarity criteria. This was accomplished by starting from the sequence of Cox11 from yeast *Saccharomyces cerevisiae* and performing a protein-protein BLAST (16) search (www.ncbi.nlm.nih.gov/BLAST/). Sequence alignments were done with ClustalW (17). The prediction of trans-membrane helices and membrane topology of Cox11 sequences is obtained using HMMTOP and TMpred programs (18, 19).

Protein and NMR Sample Preparation—The genes coding Cox11 proteins from *Agrobacterium tumefaciens*, *Caulobacter crescentus*, *Pseudomonas aeruginosa*, *R. sphaeroides*, and *S. meliloti* were selected for protein expression and amplified by polymerase chain reaction using specific primers and genomic DNA from the selected bacteria. All of the constructs lack the N-terminal trans-membrane-spanning helix. Amplified genes were cloned in pET21a expression vectors producing both native and C-terminal His_6-tagged proteins. All of the constructs were screened for expression in Luria-Bertani-ampicillin medium using BL21(DE3) *Escherichia coli* strains. The cells were grown at 37 °C, and induction was performed by isopropyl-β-D-thiogalactopyranoside. Cox11 protein from *S. meliloti* then was selected because it is mainly present in the supernatant at variance with all of the other protein constructs and showed the highest expression level. Purification of Cox11 from *S. meliloti* is performed by anionic exchange chromatography followed by size-exclusion chromatography at 4 °C. For the overexpression of ^{15}N- and $^{13}C/^{15}N$-enriched Cox11, cells were grown in minimal medium containing 0.4% of ^{13}C D-glucose and/or 0.1% $(^{15}NH_4)_2SO_4$. Protein concentration was determined by using an extinction coefficient of 13,490 M^{-1} cm^{-1} at 280 nm. Electrospray ionization-mass spectrometry spectra of apoCox11, previously reduced by DTT, were taken with an Applied Biosystems electron spray ionization-time-of-flight Mariner mass spectrometer. Analytical gel filtration was performed on a Superdex 75 10/30 HR sizing column in 20 mM phosphate buffer, pH 7, or 50 mM Tris/MES, pH 7.0, containing 5 or 1 mM DTT when specified.

Copper(I) was added as $[Cu(I)(CH_3CN)_4]PF_6$ in a 2-fold excess to apoprotein samples previously incubated with 10 mM DTT in 50 mM Tris/MES, pH 8, under a N_2 atmosphere chamber. The excess of copper was removed through a Q-Sepharose column. Copper content was checked through atomic absorption measurements with a PerkinElmer 2380 instrument. NMR samples were in 20 mM potassium phosphate buffer, pH 7, with 10% D_2O. The apoprotein concentration of NMR samples ranged from 1 to 2 mM in the presence of 5 mM DTT to prevent possible disulfide formation as more than one cysteine are present. The Cu(I) protein concentration of NMR sample was 0.5 mM in 50 mM Tris/MES buffer at pH 7.2. NMR measurements were also performed on a Cu(I)Cox11 sample containing 1 mM DTT.

NMR Spectroscopy and Structure Calculations—The NMR spectra were acquired at 298 K on Avance 800, 600, and 500 Bruker spectrometers operating at proton nominal frequencies of 800.13, 600.13, and 500.13 MHz, respectively. The NMR experiments used for the backbone and the aliphatic side chain resonances assignment and for obtaining structural restraints, recorded on $^{13}C/^{15}N$- and ^{15}N-enriched and unlabeled apoCox11 samples, are summarized in Supplemental Table I. The ^1H, ^{13}C, and ^{15}N resonance assignments of apoCox11 are reported in Supplemental Table 2. Distance constraints for structure determination were obtained from ^{15}N-edited and ^{13}C-edited three-dimensional NOESY-HSQC experiments and from two-dimensional NOESY. Backbone dihedral ϕ and ψ angles were determined through HNHα and three-dimensional ^{15}N-edited NOESY-HSQC experiments, respectively, as reported previously (20, 21). The elements of secondary structure were determined on the basis of the chemical shift index (22), of the $^3J_{HNH\alpha}$ coupling constants, and of the backbone NOEs. An automated CANDID approach combined with the fast DYANA torsion angle dynamics algorithm (23) was used to assign the ambiguous NOE cross-peaks and to have a preliminary protein structure. Structure calculations were then performed through iterative cycles of DYANA (24) implemented with the use of Ramachandran potentials (25) followed by restrained energy minimization with AMBER 5.0 (26) applied to each member of the final DYANA family. The assessment of the structures was evaluated using the programs PROCHECK-NMR (27) and AQUA (27, 28). Fold similarities in the Protein Data Bank were searched using the DALI (29), SCOP (30), and CATH (31) programs.

A structural model of the soluble domain of human Cox11, which shows a high sequence identity with Cox11 from *S. meliloti* (44%), was calculated with the program MODELLER, version 4.0 (32). Due to the high sequence identity, the structural model is expected to have a very high accuracy as validated by the PROSA energetic parameters (33).

^{15}N R_1, R_2, and steady-state heteronuclear NOEs were measured with pulse sequences as described by Farrow *et al.* (34). R_2 were measured using a refocusing time of 450 μs. In all of the experiments, the water signal was suppressed with a "water flipback" scheme (35). The experimental relaxation rates were used to map the spectral density function values, $J(\omega_H)$, $J(\omega_N)$, and $J(0)$ following a procedure available in literature (36).

X-ray Absorption Spectroscopy (XAS) Data Collection and Analysis—Two Cu(I)Cox11 samples from different protein batches have been prepared for XAS measurements to check the reproducibility of the spectrum. Each sample consisted of a 1 mM protein solution in 50 mM Tris/MES buffer at pH 7.2. Each sample was prepared under nitrogen atmosphere, and all of the subsequent handling was always conducted under inert atmosphere. The protein sample was loaded into a plastic cell covered with Kapton windows, which was carefully washed with an 100 mM EDTA solution, rinsed with pure water and absolute ethanol, and dried. The sample cell was then mounted in a two-stage Displex cryostat (modified Oxford instruments) and kept at 20 K during data collection.

XAS data were collected in fluorescence mode at the EMBL bending magnet beamline D2 (DESY, Hamburg, Germany) equipped with a Si(111) double crystal monochromator, a focusing mirror and a 12-element Ge solid-state detector. The XAS scans covered the energy range from 8725 to 9875 eV using variable energy step widths. In the x-ray absorption near-edge structure and EXAFS regions, the steps of 0.3 and 0.4–1.2 eV were used, respectively. The DORIS-III storage ring was operating at 4.5 GeV with 90–140 mA of ring current. Ionization chambers in front and behind the sample were used to monitor the beam intensity. The Bragg reflections of a static Si(220) crystal in back-reflection geometry have been used for the absolute energy calibration of the copper spectra (37). Harmonic rejection was ensured by an energy cut-off of the focusing mirror and a monochromator detuning to 60% of the peak intensity. Dead time correction was applied.

For the first Cu(I)-Cox11 sample, only nine scans could be collected, whereas for the second sample, 19 scans were collected. The individual scans were summed and averaged before data reduction, which was performed with the EXPROG software package (designed by H. F. Nolting and C. Hermes, H. F. EMBL, Hamburg, Germany). The XAS spectra from the two samples are identical within the experimental noise, and their analysis provides the same results. The reported spectrum and data analysis refer to the second (19 scans) higher quality dataset, which shows a better signal/noise ratio. The full k^3-weighted EXAFS spectrum (30–850 eV above E_0 = 8983.6 eV) and its Fourier transform calculated over the range 3.0–15.0 $Å^{-1}$ have been compared with theoretical simulations with program EXCURVE9.20 (38). The Fermi energy offset was refined at the beginning of the simulation and then kept fixed at −8.6 eV. A fixed amplitude reduction factor of 0.9 was used to compensate for the signal amplitude reduction due to multiple excitations. Ligand types and coordination numbers (kept as integers) were varied manually while distances and Debye-Waller factors were refined by the software. The quality of the fit was assessed by the parameter ϵ^2 (39) and by the *R*-factor as defined within EXCURVE9.20 (38).

Data Deposition—Resonance assignments and the derived atomic coordinates for a family of acceptable structures and for the average minimized structure with all of the restraints used in structure determination are available at the Protein Data Bank (codes 1SO9 and 1SP0).

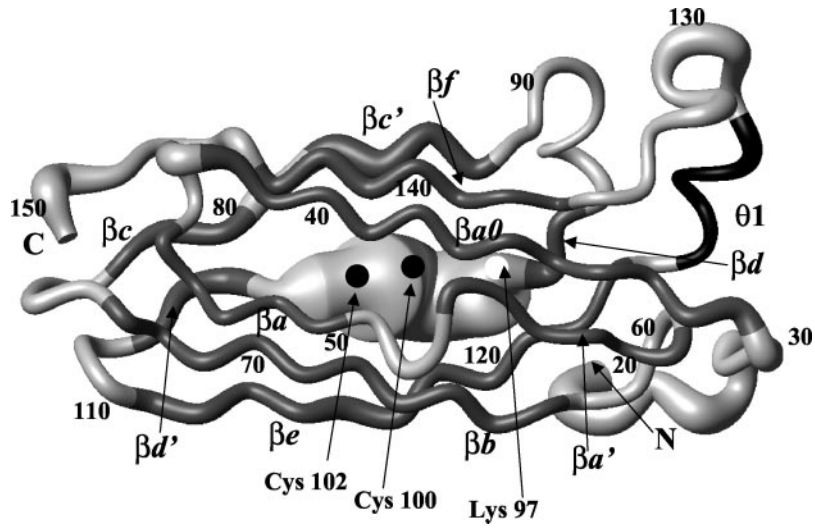

FIG. 1. **Solution structure of apoCox11 (residues 20–151).** The radius of the tube is proportional to the backbone root mean square deviation of each residue. The secondary structure elements are shown (β-strands in *gray* and helices in *black*). The two *black spheres* indicate the sulfur atoms of Cys-100 and Cys-102, whereas the *white sphere* represents the Nζ of Lys-97.

RESULTS

Genome Browsing and Expression of Cox11 from S. meliloti—A BLAST search over all of the non-redundant GenBank™ genomes for proteins sharing >10% sequence identity with the amino acid sequence of Cox11 from yeast *S. cerevisiae* located 49 protein sequences. All of the searched sequences belong only to Gram-negative bacterial or to eukaryotic organisms. The Cox11 sequences have quite a variable length, but for a common region, a high average residue identity of 36 ± 8% was found, indicating a highly conserved protein family. A possible metal binding motif CFCF (not used in the search) is conserved in all of the sequences (Supplemental Fig. 1). A third cysteine at the N terminus at position 43 proposed to be involved in copper(I) binding in yeast Cox11 (15) is conserved in all of the sequences with the exception of three (Supplemental Fig. 1). A Lys residue at position 131 close to the metal binding motif CFCF is also fully conserved (Supplemental Fig. 1). A hydropathy analysis indicates that this class of proteins contains a single N-terminal trans-membrane-spanning helix, suggesting that they are membrane-bound proteins and that a water-soluble segment can be produced if the N-terminal trans-membrane segment is taken out. This soluble segment entirely comprises the highly conserved amino acids region previously mentioned.

Sequences from five different bacterial organisms were selected to express the protein. The organisms are as follows: *S. meliloti*; *R. sphaeroides*; *A. tumefaciens*; *C. crescentus*; and *P. aeruginosa*. Protein cloning was successfully performed on all of the selected protein sequences, yielding both C-terminal His tag fusion proteins and native untagged proteins. Expression of all of the His tag constructs yielded non-soluble proteins mainly present in the pellet as inclusion bodies while being in the supernatant only upon the addition of 4–6 M urea. Regarding the untagged constructs, the protein from *S. meliloti* is largely present in the supernatant and shows high expression levels; therefore, it was selected for the following structural study.

The Cox11 gene from *S. meliloti* codes for a protein of 198 amino acids. The single N-terminal trans-membrane-spanning helix involves residues from Gly-15 to Val-36. Therefore, we expressed a recombinant protein, Cox11, lacking the first 35 residues and thus being 164-amino acids-long (including the first Met residue inserted for the cloning procedure). After the purification steps, the protein does not contain any heavy metal ion. ESI-mass spectrometry spectra show the presence of two species in solution with masses of 18,371 and 18,140 Da, which correspond, respectively, to the cloned construct of 164 amino acids and to a construct where the first two residues, Met-1 and Val-2, were absent (residue numbering is based on the former construct). Analytical gel-filtration analysis showed that apoCox11 eluted in fractions corresponding to a monomeric state when 5 mM DTT was present in the buffer (subsequently confirmed by ^{15}N relaxation measurements) with a little fraction of a dimeric form. When DTT was removed from the eluting buffer, apoCox11 eluted primarily as a dimer with a fraction of protein consistently appearing as higher order aggregates. This behavior suggests that protein dimerization could occur through the formation of one or more intermolecular disulfide bonds.

Structural and Dynamic Characterization of ApoCox11—The ^{1}H-^{15}N and ^{1}H-^{13}C HSQC spectra of apoCox11 show well dispersed resonances indicative of an essentially folded protein. 134 of the expected 152 ^{15}N backbone amide resonances were assigned for apoCox11 in the presence of 5 mM DTT. The amide resonances are missing for residues 1–10 and 97–105. In total, the resonances of 92% carbon atoms, 93% nitrogen atoms, and 90% protons (calculated considering the segments 11–96 and 106–164) were assigned. Chemical shift index analysis (22) on Hα, CO, Cα, and Cβ resonances, $^{3}J_{HNH\alpha}$ coupling constants, $d_{\alpha N}$(i-1,i)/$d_{N\alpha}$(i,i) ratios (21) and NOEs patterns indicated the presence of 10 β-strands and a 3_{10} helix.

By analyzing three-dimensional ^{15}N-edited and ^{13}C-edited NOESY spectra and two-dimensional NOESY spectra, 6733 NOE cross-peaks were assigned and transformed into 3771 unique upper distance limits of which 2867 were meaningful (Supplemental Fig. 2). 66 ϕ- and 64 ψ-dihedral angle restraints were determined. After restrained energy minimization on each of the 30 conformers of the family, the root mean square deviation of the mean structure was 0.69 Å (with a variability of 0.10 Å) and 1.16 Å (with a variability of 0.10 Å) for the backbone and heavy atoms, respectively (Supplemental Fig. 2), when the N- and C-terminal segments 11–20 and 152–164 and the unassigned residues 97–105 were not included. The final restrained energy minimization family has a target function of 0.35 ± 0.04 Å^2 and 0.14 ± 0.05 rad^2 for the NOEs and the dihedral angle constraints, respectively. The results of the conformational and energetic analysis of the final restrained energy minimization family of apoCox11 are reported in Supplemental Table III. The solution structure of apoCox11 shown in Fig. 1 is formed by the following secondary structure elements: $\beta a0$-(31–42); βa-(46–50); $\beta a'$-(54–59); $\beta b'$-(64–73); $\beta c'$-(78–80); $\beta c'$-(83–86); $\beta d'$-(95–96); $\beta d'$-(106–108); βe-(112–122); helix $3_{10}(\theta 1)$-(124–128); and βf-(138–144). The 10 β-strands are organized with parallel and antiparallel alignments to form an almost β-barrel structure constituted by two layers of β-sheets.

One sheet is formed by strands βa, βb, βe, βd, and the other sheet is formed by strands βa′, βa0, βf, and βc′ (Fig. 1). In addition, strands βc and βd′ form a short antiparallel β-sheet. The most disordered regions are those involving residues 96–105 and the N and C termini, which show random coil conformation as the chemical shift index values indicate.

^{15}N R_1, R_2, and ^1H-^{15}N NOE values can provide information on internal mobility as well as on the overall protein tumbling rate. From the analysis of 112 backbone NH signals, which are well resolved in the ^1H-^{15}N apoCox11 spectra, average R_1, R_2, and ^1H-^{15}N NOE values of 1.72 ± 0.06, 12.7 ± 0.5, and 0.60 ± 0.05 s^{-1} are found, respectively, at 600 MHz. The experimental relaxation data (Supplemental Fig. 3) are essentially homogenous along the entire polypeptide sequence with the exception of residues located at the C and N termini. The correlation time for the molecule tumbling (τ_m) as estimated from the R_2/R_1 ratio is 8.8 ± 0.6 ns as expected for a protein of this size in a monomeric state (40, 41), thus confirming the results from the gel-filtration analysis. From the spectral density function analysis (Supplemental Fig. 4), it appears that the residues at the N and C termini experience local motions in the sub-ns timescale, *i.e.* faster than the overall protein tumbling rate. The occurrence of sub-ns motions for residues belonging to the N- and C-terminal regions can explain the paucity of NOEs in these regions, thus determining their high root mean square deviation values.

Interaction with Copper: XAS and NMR Characterization—To characterize copper(I) binding to *S. meliloti* Cox11, the purified apoprotein was treated with an excess of $[Cu(I)(CH_3CN)_4]PF_6$ (see "Experimental Procedures"). The produced Cu(I)·Cox11 complex is stable only in dilute solution. At a high concentration, the protein starts to form a brown gelatinous precipitate. Atomic absorption spectroscopy showed that Cox11 from *S. meliloti* binds approximately one copper atom per monomer as found for yeast Cox11 (15). The ^1H-^{15}N HSQC spectra of apoCox11 and Cu(I)·Cox11 show sizable chemical shift variations for residues 83–86, 96, and 106 (Supplemental Fig. 5), whereas the CFCF metal-binding region still elude detection, possibly because of line-broadening due to conformational exchange processes. A similar phenomenon was already observed for Cu(I)-CopZ from *Enterococcus hirae* (42). It is important to notice that the observed chemical shift changes are localized in the β-strands spatially closest to the CFCF copper-binding region. In addition, even in the presence of copper(I) ion, the N and C termini are not rigidified as NH signals of residues 12–20 and 154–164 are not observed and no significant chemical shifts are observed for the closer residues. The ^{15}N relaxation rates, measured on a Cu(I)·Cox11 sample containing 1 mM DTT at 500 MHz, provide average values for R_1 and R_2 of 1.47 ± 0.05 and 19.6 ± 0.8 s^{-1}, respectively. The R_2 values overall show a sizable increase with respect to apoCox11, whereas the R_1 values show a global decrease. The correlation time τ_m of Cu(I)·Cox11 is 14.7 ± 1.0 ns, consistent with a predominantly dimeric state of the copper(I)-loaded form. A similar correlation time was also obtained when DTT was removed from the buffer. The same behavior is observed in the gel-filtration analysis where the Cu(I)·Cox11 complex is predominantly found in a dimeric state as it also occurs for yeast Cox11 (15).

X-ray absorption spectroscopy on *S. meliloti* Cu(I)·Cox11 shows, in the K-edge region, the presence of an absorption at 8983.9 eV (Supplemental Fig. 6*A*). This band is assigned to a 1s → 4p transition in the copper(I) compounds (43), thus clearly confirming the copper oxidation state as Cu(I). The height of the 1s → 4p transition suggests a three- or four-coordination for Cu(I) (44, 45). The EXAFS and the Fourier transform spectra of *S. meliloti* Cu(I)·Cox11 (Supplemental Fig. 6, *B* and *C*) are well reproduced by the presence of three sulfur atoms at 2.23 Å in the first coordination shell of the Cu(I) ion (Supplemental Table IV, *Fit 2*). This distance is typical of 3-coordinated Cu(I) complexes (43, 44). Attempts to fit the copper first coordination shell with two or four sulfur atoms lead to unrealistic fits (Supplemental Table IV, *Fits 1* and *3*). The presence of a higher frequency component of the EXAFS spectrum is revealed by the distinct second shell peak present at ~2.7 Å in the spectrum Fourier transform (Supplemental Fig. 6*C*). The peak height is defined above noise and can be well simulated by a second copper backscatterer located at 2.70–2.71 Å (Supplemental Table IV, *Fit 4*). On the contrary, a shell of 1–5 light atoms (C/N/O/S) was unable to reproduce that feature (for example see Supplemental Table IV, *Fit 5*). The position and the height of this peak do not change if the Fourier transform is performed over a different *k*-range, suggesting that this peak is a real component of the spectrum. The high Debye-Waller factor ($2\sigma^2$ = 0.021 Å^2) suggests the presence of static disorder in the Cu environment. Indeed, splitting the 3-S shell in two different distances resulted in a significant improvement of the fit when 1 S at a shorter distance and 2 S at a longer distance were used for the spectrum simulation, providing an excellent fit with 1 S at 2.19 Å, 2 S at 2.24 Å, and 1 Cu at 2.70 Å (Supplemental Table IV, *Fits 6* and *7*). The same Cu(I) coordination (*i.e.* 3 S at 2.24 Å and 1 Cu at 2.70 Å) has been observed in yeast Cox11 for which Cys residues are involved in copper binding (15). The distance of 2.7 Å is in accordance with Cu-Cu distances observed in doubly bridging sulfur complexes, which range from 2.7 to 3.0 Å, whereas the Cu-Cu distances in singly bridged sulfur clusters are around 3.3 Å (45, 46). Similar EXAFS data were also found for Cu(I)-CopZ samples, indicating a common copper binding motif (47).

All of the experimental data on Cu(I)·Cox11 from *S. meliloti* indicate that copper(I) is bound to three sulfur atoms of Cys ligands organized in a binuclear cluster at the interface of the dimerization side.

DISCUSSION

Genome browsing for Cox11 homologues individualizes a highly conserved protein family present exclusively in eukaryotes and in Gram-negative bacteria. The available functional data indicate that Cox11 is restricted to a specific function in the CcO complex assembly mechanism (14). Its structure determination represents an essential step to unravel its functional role. The overall structure of the soluble domain of apoCox11 reveals a compact well defined domain composed entirely of β strands, either parallel or antiparallel. The 10 β-strands are connected by an extensive backbone hydrogen bond network, thus forming an almost cylindrical β-barrel. Some of the β-strands are separated by short loops containing in some cases highly conserved residues of "special" conformational properties such as Gly or Pro, which can impart a shift to the strand position. This property makes strands βa and βa′, which are separated by a highly conserved proline (Pro-51), form hydrogen bonds with strands βb and βa0, respectively. The highly disordered copper-binding region containing Cys-100 and Cys-102 as ligands is located between two short β strands (βd and βd′), which form two different antiparallel β-sheets with strands βe and βc, respectively.

The core of apoCox11 structure is characterized by several hydrophobic interactions, which involve buried aromatic and aliphatic residues located in 9 of the 10 β-strands. This hydrophobic core is highly conserved in all of the bacterial and eukaryotic Cox11 homologous proteins (Supplemental Fig. 1), whereas the N- and C-terminal segments are characterized by a large variability in length as well as the nature of the amino

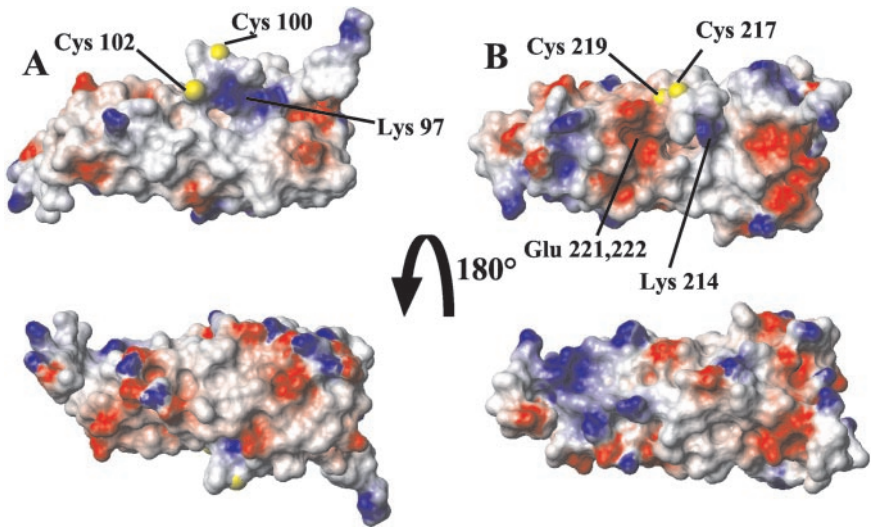

FIG. 2. **Rotated views of the electrostatic surfaces of Cox11.** Rotated views of *S. meliloti* Cox11 (*A*) and human Cox11 (*B*) are shown. The positively, negatively charged, and neutral amino acids are represented in *blue*, *red*, and *white*, respectively. The positions of the sulfur atoms of Cys residues are indicated as *yellow spheres*. The position of other relevant residues is also indicated.

acids with the exception of few residues close to the transmembrane helix. In accordance, the structural characterization shows that the N- and C-terminal regions are not able to make hydrophobic contacts to get structured. Consequently, the possible copper ligand Cys-9 is located in a completely unstructured part of apoCox11, whereas the other potential copper ligands located in the conserved motif CFCF are inserted in the β-barrel structure.

The side of *S. meliloti* Cox11 structure, which contains the putative copper binding motif CFCF is highly hydrophobic with the exception of the adjacent positive charge of the fully conserved Lys-97 (Fig. 2*A*). The proximity of Lys-97 can counterbalance the overall negative charge produced by cysteine ionization when binding of Cu(I) occurs. Indeed, in Cu(I)Atx1 from *S. cerevisiae*, the approach of a conserved positively charged residue, Lys-65, to the copper site upon copper binding represents a structural rearrangement that optimizes electrostatic interactions (48). The surface of the human Cox11 model displays a negative patch close to the copper binding motif CFCF, which is produced by two Glu residues (Fig. 2*B*), highly conserved in only eukaryotic organisms (Supplemental Fig. 1). This different charged distribution between bacterial and eukaryotic organisms could suggest that the negative patch close to the copper-binding region is important in eukaryotes for the interaction of Cox11 with the proposed copper chaperone partner, Cox17, which is indeed not present in any bacteria. To support the latter hypothesis, it should be noticed that even the other proposed protein partner of Cox17, Sco1, contains two negative charged residues close to the copper(I) binding motif C*XXX*CP, which are analogous to Cox11 sequences highly conserved in eukaryotes but not in bacteria.

Structural homologies and Mechanistic Implications—Within proteins adopting a fold similar to that of apoCox11, the closest matches are with immunoglobulin-like domains. In particular, the search identified two structurally related proteins, *i.e.* a linker domain of a bacterial sialidase (Protein Data Bank code 1eut) and a motile major sperm protein of *Ascaris suum* (Protein Data Bank code 1msp) (Fig. 3). Cox11 from *S. meliloti* shares with the two above-mentioned proteins only a 10 and 13% residue identity, respectively.

Ig-like domains are classified into five subtypes (C, V, I, S, and H) according to the number of strands and the H-bond interactions between them (49). Backbone hydrogen-bonding patterns in the Ig-like domains define two sheets organized in a β-sandwich-fold, rather than a closed barrel. All of the Ig-like domains have a common core of six β-strands: β*a*, β*b*, and β*e* in one sheet and β*c*, β*f*, and β*g* in the other (*colored gray* in Fig. 3). However, apoCox11 protein, despite a closely related fold, shows different structural features, which lead us to classify it as the prototype for a new class of Ig-related domain. Indeed, by comparing apoCox11 with the two closest structurally Ig proteins (Fig. 3), it appears that apoCox11 at the N terminus has an additional β-strand, β*a*0, which forms a parallel β-sheet with β*f*. Strand β*a*0 replaces, but in an opposite direction, the "Ig" strand β*g*, which is present at the C terminus in all of the Ig-related domains, and always forms antiparallel β-sheet with strand β*f*. On its turn, strand β*f* is interacting with strand β*c* in all of the Ig structures, thus forming a completely conserved three-stranded β-sheet. On the contrary, in the apoCox11 structure, the Ig strand β*c* is divided by a short loop into strands β*c* and β*c*′ (Fig. 3). Therefore, in this new subtype of Ig-like domains, the Ig-conserved β*g*, β*f*, and β*c* sheet is now formed by strands β*a*0, β*f*, and β*c*′ (Fig. 3).

It is known that Ig-like fold occurs in functionally diverse proteins, but in most cases, the common denominator is a recognition role at the cell surface (50, 51). This family of molecules is of fundamental importance in the immune system and in the intracellular recognition (50). The Ig-related molecules commonly form dimers to carry out their function, forming either a homodimer or heterodimers (50). A specific class of Igs called CD8 are dimers linked by an intermolecular disulfide bond present after a C-terminal trans-membrane helix, which is then followed by the one or more Ig-soluble domains (52–54). Apparently, any accessible part of the Ig domain surface can be involved in interactions with other molecules (50, 51). In few examples, the Ig-fold family is involved in metal binding and the metal binding sites are essentially located in the loops at the edges of the β-sandwich (55). In the Cox11 structure, the copper binding motif is inserted differently in the β-sheet region. This peculiar structural feature might be the factor determining the different functions of Cox11 with respect to those of Ig-like proteins. Indeed, the function of Cox11 is related to Cu_B site formation, possibly delivering copper directly to that site. *In vitro*, Cox11 is capable of binding copper(I) forming at the interface of the dimerization domain, a binuclear copper(I) cluster, as indicated by the EXAFS data of Cu(I)Cox11. The formation of the copper(I) cluster could occur transiently in the cell and could be a response to the need for copper to reach a more energetically stable coordination. Indeed, copper(I) prefers three-coordination geometry, and when endogenous ligands are not available, it saturates its coordination sphere by binding an exogenous ligand as glutathione or sharing a ligand with another protein molecule, thus producing a dimer. A reasonable model for the copper site of the dimeric state of

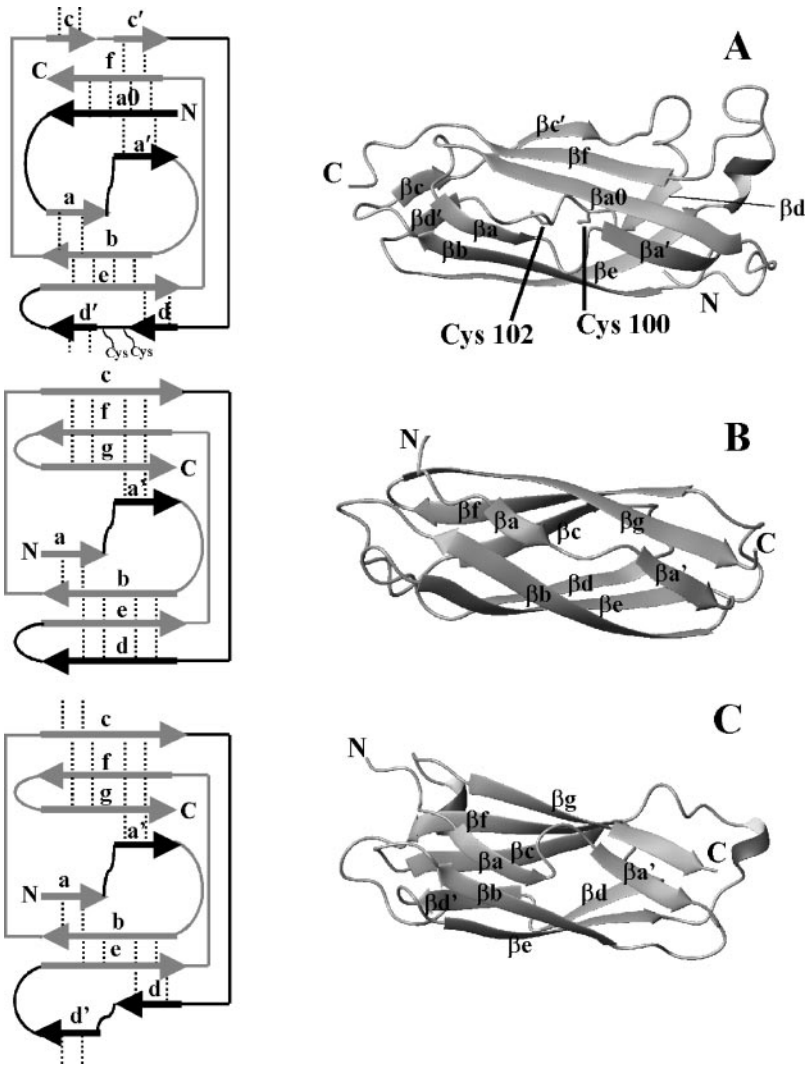

FIG. 3. **Comparison between the structures and the two-dimensional topology of apoCox11 (*A*), a linker domain of a bacterial sialidase (Protein Data Bank code 1eut) (*B*), and a motile major sperm protein of *A. suum* (Protein Data Bank code 1msp) (*C*).** The side chains of the Cys-100 and Cys-102 are indicated. The *dashed lines* indicate sheet formation between two β-strands. β-Strands a, b, c, e, f, and g (*colored gray*) are common to all of the Ig-like domains.

Cu(I)·Cox11 contains one cysteine residue (Cys-100 or Cys-102) from each monomer acting as a monodentate ligand to one copper and one cysteine (Cys-100 or Cys-102) acting as a bridging bidentate ligand to both copper ions (Fig. 4). Indeed, the observed Cu-Cu distance of 2.7 Å is typical of doubly bridging sulfur complexes (56, 57) and was found in other copper(I) chaperones with similar rearrangements (45, 58). The N-terminal Cys-9, which is located far from the CFCF binding site and in an unstructured region only five/four residues of the inner membrane, would not be involved in copper binding but rather could be involved in an intermolecular disulfide bond with the corresponding cysteine of the other monomeric unit (Fig. 4). Indeed, the same occurs in the structurally related Ig CD8-dimeric protein, which dimerizes through the S–S bond (53, 54). This intermolecular disulfide bond can be essential for the *in vivo* function, thus explaining the respiratory incompetence observed in the yeast Cys-111 → Ala variant (15).

It is relevant to mention that also the apoform in the absence of reductant is predominantly in a dimeric state. The similar tendency to form a dimer, observed for both eukaryotes (yeast) (15) and for bacteria (*S. meliloti*), suggests that this self-aggregation process is mainly determined by the fold properties and/or by the possibility of intermolecular S–S bond formation, more than from electrostatic interaction, which should be minimal for eukaryotic proteins characterized by extensive negative regions close to the metal binding motif. The tendency to dimerize apoCox11, typical of most Ig-fold proteins, might play

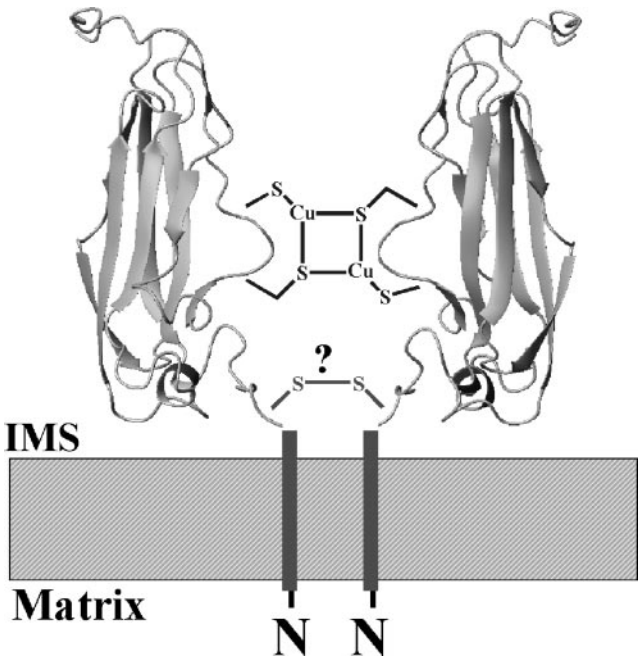

FIG. 4. **Model for the Cu(I)Cox11-dimeric form.** The binuclear copper(I) cluster involving the CFCF copper binding motif and the proposed disulfide bond involving Cys-9 are shown. *IMS*, intermembrane space.

a role in the process of copper binding, *i.e.* taking two protein molecules close each other to receive copper ion.

The flexibility of copper(I) coordination is known to be relevant for the copper transfer process (59–61). Assuming that Cox11 directly transfers the metal to COX I subunit, the copper transfer could occur in a heterodimeric complex where two different metal environment are present: 1) all-sulfur ligands in Cox11 and 2) all-nitrogen ligands in COX I. Analogously, this occurs in the copper transfer between the dimeric copper chaperone copper chaperone for superoxide dismutase containing a copper(I) binuclear cluster similar to Cu(I)Cox11 (45) and its protein target, the dimeric superoxide dismutase, where four His residues coordinate the copper ion (62). Therefore, it might be suggested that the dimeric state of Cox11 may stabilize copper binding, protecting the copper until transfer to COX I occurs. It was proposed that mitochondrial ribosomal proteins could be involved in signaling to Cox11 the incoming translation of COX I (1), and concomitantly to the latter process, Cox11 may disrupt the dimer to form a heterodimer with COX I, thus inserting the copper ion in the Cu_B site.

All of these considerations indicate a reasonable functional role of a dimeric Cu(I)·Cox11 intermediate in this intriguing mechanism of copper delivery to the membrane protein CcO, which is generally assumed to be a dimeric complex *in vivo* (63, 64).

Acknowledgments—We thank Prof. R. Udisti for atomic absorption spectroscopy and Prof. G. Moneti for carrying out the mass spectrometry experiments. We also thank Elena Bacci for preparing the protein samples.

REFERENCES

1. Carr, H. S., and Winge, D. R. (2003) *Acc. Chem. Res.* **36,** 309–316
2. O'Halloran, T. V., and Culotta, V. C. (2000) *J. Biol. Chem.* **275,** 25057–25060
3. Nobrega, M. P., Bandeira, S. C. B., Beers, J., and Tzagoloff, A. (2002) *J. Biol. Chem.* **277,** 40206–40211
4. Glerum, D. M., Shtanko, A., and Tzagoloff, A. (1996) *J. Biol. Chem.* **271,** 14504–14509
5. Tzagoloff, A., Capitanio, N., Nobrega, M. P., and Gatti, D. (1990) *EMBO J.* **9,** 2759–2764
6. Glerum, D. M., Shtanko, A., and Tzagoloff, A. (1996) *J. Biol. Chem.* **271,** 20531–20535
7. Schulze, M., and Rodel, G. (1988) *Mol. Gen. Genet.* **211,** 492–498
8. Tzagoloff, A., and Dieckmann, C. L. (1990) *Microbiol. Rev.* **54,** 211–225
9. Lode, A., Kuschel, M., Paret, C., and Rodel, G. (2000) *FEBS Lett.* **485,** 19–24
10. Dickinson, E. K., Adams, D. L., Schon, E. A., and Glerum, D. M. (2000) *J. Biol. Chem.* **275,** 26780–26785
11. Mattatall, N. R., Jazairi, J., and Hill, B. C. (2000) *J. Biol. Chem.* **275,** 28802–28809
12. Mogi, T., Saiki, K., and Anraku, Y. (1994) *Mol. Microbiol.* **14,** 391–398
13. Barros, M. H., Carlson, C. G., Glerum, D. M., and Tzagoloff, A. (2001) *FEBS Lett.* **492,** 133–138
14. Hiser, L., Di Valentin, M., Hamer, A. G., and Hosler, J. P. (2000) *J. Biol. Chem.* **275,** 619–623
15. Carr, H. S., George, G. N., and Winge, D. R. (2002) *J. Biol. Chem.* **277,** 31237–31242
16. Altschul, S. F., Madden, T. L., Schaeffer, A., Zhang, J., Zhang, Z., Miller, W., and Lipman, D. J. (1997) *Nucleic Acids Res.* **25,** 3389–3402
17. Thompson, J. D., Higgins, D. G., and Gibson, T. J. (1994) *Nucleic Acids Res.* **22,** 4673–4680
18. Hofmann, K., and Stoffel, W. (1993) *Biol. Chem. Hoppe-Seyler* **347,** 166–170
19. Tusnady, G. E., and Simon, I. (1998) *J. Mol. Biol.* **283,** 489–506
20. Vuister, G. W., and Bax, A. (1993) *J. Am. Chem. Soc.* **115,** 7772–7777
21. Gagne, R. R., Tsuda, S., Li, M. X., Chandra, M., Smillie, L. B., and Sykes, B. D. (1994) *Protein Sci.* **3,** 1961–1974
22. Wishart, D. S., and Sykes, B. D. (1994) *J. Biomol. NMR* **4,** 171–180
23. Herrmann, T., Güntert, P., and Wüthrich, K. (2002) *J. Mol. Biol.* **319,** 209–227
24. Güntert, P., Mumenthaler, C., and Wüthrich, K. (1997) *J. Mol. Biol.* **273,** 283–298
25. Bertini, I., Cavallaro, G., Luchinat, C., and Poli, I. (2003) *J. Biomol. NMR* **4,** 355–366
26. Pearlman, D. A., Case, D. A., Caldwell, J. W., Ross, W. S., Cheatham, T. E., Ferguson, D. M., Seibel, G. L., Singh, U. C., Weiner, P. K., and Kollman, P. A. (1997) *AMBER 5.0*, University of California, San Francisco
27. Laskowski, R. A., Rullmann, J. A. C., MacArthur, M. W., Kaptein, R., and Thornton, J. M. (1996) *J. Biomol. NMR* **8,** 477–486
28. Laskowski, R. A., MacArthur, M. W., and Thornton, J. M. (1998) *Curr. Opin. Struct. Biol.* **8,** 631–639
29. Holm, L., and Sander, C. (1996) *Science* **273,** 595–603
30. Murzin, A. G., Brenner, S. E., Hubbard, T., and Clothia, C. (1995) *J. Mol. Biol.* **247,** 536–540
31. Orengo, C. A., Michie, A. D., Jones, S., Jones, D. T., Swindells, M. B., and Thornton, J. M. (1997) *Structure* **5,** 1093–1108
32. Sali, A., and Blundell, T. L. (1993) *J. Mol. Biol.* **234,** 779–815
33. Sippl, M. J. (1993) *Proteins Struct. Funct. Genet.* **17,** 355–362
34. Farrow, N. A., Muhandiram, R., Singer, A. U., Pascal, S. M., Kay, C. M., Gish, G., Shoelson, S. E., Pawson, T., Forman-Kay, J. D., and Kay, L. E. (1994) *Biochemistry* **33,** 5984–6003
35. Grzesiek, S., and Bax, A. (1993) *J. Am. Chem. Soc.* **115,** 12593–12594
36. Peng, J. W., and Wagner, G. (1992) *J. Magn. Reson.* **98,** 308–332
37. Pettifer, R. F., and Hermes, C. (1985) *J. Appl. Crystallogr.* **18,** 404–412
38. Binsted, N., and Hasnain, S. S. (1996) *J. Synchrotron Radiat.* **3,** 185–196
39. Lytle, F. W., Sayers, D. E., and Stern, E. A. (1989) *Phys. Rev. B* **11,** 2795–2801
40. Stokes, G. (1956) *Trans. Cambridge Philos. Soc.* **9,** 5–10
41. Einstein, A. (1956) *Investigations on the Theory of the Brownian Movement*, Dover, New York
42. Wimmer, R., Herrmann, T., Solioz, M., and Wüthrich, K. (1999) *J. Biol. Chem.* **274,** 22597–22603
43. Pickering, I. J., George, G. N., Dameron, C. T., Kurz, B., Winge, D. R., and Dance, I. G. (1993) *J. Am. Chem. Soc.* **115,** 9498–9505
44. Blackburn, N. J., Strange, R. W., Reedijk, J., Volbeda, A., Farooq, A., Karlin, K. D., and Zubieta, J. (1989) *Inorg. Chem.* **28,** 1349–1357
45. Eisses, J. F., Stasser, J. P., Ralle, M., Kaplan, J. H., and Blackburn, N. J. (2000) *Biochemistry* **39,** 7337–7342
46. Srinivasan, C., Posewitz, M. C., George, G. N., and Winge, D. R. (1998) *Biochemistry* **37,** 7572–7577
47. Banci, L., Bertini, I., Del Conte, R., Mangani, S., and Meyer-Klaucke, W. (2003) *Biochemistry* **8,** 2467–2474
48. Arnesano, F., Banci, L., Bertini, I., Huffman, D. L., and O'Halloran, T. V. (2001) *Biochemistry* **40,** 1528–1539
49. Halaby, D. M., Poupon, A., and Mornon, J. P. (1999) *Protein Eng.* **12,** 563–571
50. Williams, A. F., and Barclay, A. N. (1988) *Annu. Rev. Immunol.* **6,** 381–485
51. Bork, P., Holm, L., and Sander, C. (1994) *J. Mol. Biol.* **242,** 309–320
52. Leahy, D. J., Axel, R., and Hendrickson, W. A. (1992) *Cell* **68,** 1145–1162
53. Parnes, J. R. (1989) *Adv. Immunol.* **44,** 265–311
54. Zamoyska, R. (1998) *Curr. Opin. Immunol* **10,** 82–87
55. Bullock, T. L., Roberts, T. M., and Stewart, M. (1996) *J. Mol. Biol.* **263,** 284–296
56. Iwata, S., Ostermeier, C., Ludwig, B., and Michel, H. (1995) *Nature* **376,** 660–669
57. Atkinson, E. R., Raper, E. S., Gardiner, D. J., Dawes, H. M., Walker, N. P. C., and Jackson, A. R. W. (1985) *Inorg. Chim. Acta* **100,** 285–291
58. Graden, J. A., Posewitz, M. C., Simon, J. R., George, G. N., Pickering, I. J., and Winge, D. R. (1996) *Biochemistry* **35,** 14583–14589
59. Pufahl, R., Singer, C. P., Peariso, K. L., Lin, S.-J., Schmidt, P. J., Fahrni, C. J., Cizewski Culotta, V., Penner-Hahn, J. E., and O'Halloran, T. V. (1997) *Science* **278,** 853–856
60. Arnesano, F., Banci, L., Bertini, I., Cantini, F., Ciofi-Baffoni, S., Huffman, D. L., and O'Halloran, T. V. (2001) *J. Biol. Chem.* **276,** 41365–41376
61. Huffman, D. L., and O'Halloran, T. V. (2000) *J. Biol. Chem.* **275,** 18611–18614
62. Banci, L., Bertini, I., Cramaro, F., Del Conte, R., and Viezzoli, M. S. (2002) *Eur. J. Biochem.* **269,** 1905–1915
63. Klingenberg, M. (1981) *Nature* **290,** 449–454
64. Musatov, A., Ortega-Lopez, J., and Robinson, N. C. (2000) *Biochemistry* **39,** 12996–13004

Solution Structure of Cox11, a Novel Type of β-Immunoglobulin-like Fold Involved in Cu_B Site Formation of Cytochrome *c* Oxidase

Lucia Banci, Ivano Bertini, Francesca Cantini, Simone Ciofi-Baffoni, Leonardo Gonnelli and Stefano Mangani

J. Biol. Chem. 2004, 279:34833-34839.
doi: 10.1074/jbc.M403655200 originally published online June 4, 2004
